JOURNAL OF GUIDANCE, CONTROL, AND DYNAMICS
Vol. 30, No. 6, November–December 2007

New Synchronous Orbits Using the Geomagnetic Lorentz Force

Brett Streetman* and Mason A. Peck†
Cornell University, Ithaca, New York 14853

DOI: 10.2514/1.29080

The Lorentz-augmented orbits concept provides propellantless electromagnetic propulsion without a tether, using the interaction between an electrostatically charged satellite and the Earth's magnetic field to provide a useful thrust. New types of Earth-synchronous orbits are found from equations governing the motion of satellites experiencing the Lorentz force in orbit. The equations of motion for such a spacecraft are derived based on a simplified magnetic field model, in which the dipole is aligned with true north. For a polar-orbiting satellite, a constant electrical charge can create arbitrary changes in the right-ascension angle. This method allows for single-orbit repeat-groundtrack low-Earth-orbit satellites. Analytical expressions for changes in orbital elements due to Lorentz forces are verified by numerical simulation for the polar and equatorial cases. In the equatorial case, manipulation of the longitude of perigee by constant electrostatic charge is possible. Perigee movement also allows for the creation of an Earth-synchronous type of orbit. The case of a dipole field, for which the north pole is not aligned with true north, is also examined. Feedback control using only the Lorentz force for actuation is shown to stabilize this general case.

I. Introduction

IN A repeat-groundtrack orbit, the subsatellite point traces out a recurring pattern in some integer number of orbital periods. Traditionally, these orbits are achieved by adjusting the period of a satellite such that it completes an integer number of revolutions in exactly an integer number of sidereal Earth days. Geostationary and geosynchronous Earth orbits (GEOs) are perhaps the most familiar and useful examples. These orbits have a mean motion equal to the spin rate of the Earth. We shall refer to orbits that repeat their groundtrack every orbital period as GT-1 orbits. Thus, all trajectories in GEO are in the GT-1 class. A more general class, the GT-x orbit, repeats its groundtrack every x revolutions. For example, satellites in the GPS constellation are in 12 sidereal hour orbits and can thus be considered GT-2 satellites. Many low-Earth-orbit (LEO) imaging satellites designed for full-Earth coverage also use repeat-track orbits. Every 16 days, over the course of 233 orbits, Landsat 7 covers the full Earth, making it a GT-233 satellite [1]. Repeat-groundtrack Keplerian orbits are based on the number of Earth days that pass before the ground track is repeated. However, augmenting the orbit with the Lorentz force enables repeat-groundtrack orbits that are not tied to integer multiples of the Earth's spin period.

Dedicated weather satellites and both government and commercial communications satellites are just a few of the numerous uses for GT-1 orbits. However, GT-1 systems are currently limited to GEO. The altitude of these satellites, roughly 36,000 km, requires high-power communications and impacts the aperture requirements for Earth-imaging satellites. An ideal arrangement would be a GT-1 orbit at a low-Earth altitude. This paper proposes just that: a low-Earth polar GT-1 orbit achieved with propellantless propulsion. Although such an orbit is not geostationary in the sense of an equatorial GEO satellite, it is geosynchronous. The groundtrack repeats every orbital period.

The propellantless propulsion technique proposed here allows one to realize a so-called Lorentz-augmented orbit (LAO). A spacecraft capable of such an orbit behaves as a charged particle subject to interactions with the Earth's magnetic field. We begin with a summary of the elementary electrodynamics involved. The Lorentz force experienced by a particle of charge q (coulombs) moving through a magnetic field $\mathbf{B}$ is given by

$$\mathbf{F}_L = q\mathbf{v}_\mathbf{r} \times \mathbf{B} \tag{1}$$

where $\mathbf{v}_\mathbf{r}$ is the particle velocity with respect to the magnetic field. This force, named after Dutch physicist and Nobel Prize winner Hendrik Lorentz, accelerates a spacecraft that is already subject to the force of gravity, augmenting the familiar Keplerian dynamics. An LAO exploits the interaction between the Earth's geomagnetic field and an electrostatic charge built up on a satellite [2]. Thus, an LAO results from electrodynamic propulsion that does not require a tether. A tether system normally entails a long conductive wire, through which a current is forced. The drifting electrons in the tether provide the moving charged particles necessary for the Lorentz force [3]. In LAO, the spacecraft itself becomes the moving charged particle, creating a current along its orbital path.

An LAO is achieved by a spacecraft that uses electrical power to build up a net electrostatic charge on its body, and this net charge causes an interaction between the geomagnetic field and the vehicle in the form of the Lorentz force. The magnitude and direction of the force are defined by the size and polarity of the charge on the satellite q, the velocity of the vehicle with respect to the magnetic field $\mathbf{v}_r$, and the strength and direction of the magnetic field $\mathbf{B}$:

$$\mathbf{F}_L = q(\mathbf{v} - \omega_E \times \mathbf{r}) \times \mathbf{B} \tag{2}$$

where the position of the satellite is given by $\mathbf{r}$, and ω_E represents the Earth's angular velocity. In an inertial frame, the geomagnetic field rotates with the Earth [4]. The relative velocity $\mathbf{v}_r$ that causes the Lorentz force results from the difference between the absolute spacecraft velocity $\mathbf{v}$ and the velocity of the magnetic field, $\omega_\mathbf{E} \times \mathbf{r}$. The power system of the satellite can then modulate the net charge to control the propulsive force.

The LAO concept offers propellant-free propulsion. The energy stored in the Earth's rotation is used to do work on the vehicle. The size of the force is limited only by the charge-holding capacity (i.e., its self-capacitance) and available power of the satellite. However, the direction of thrust is fixed with respect to the velocity direction of the spacecraft and the direction of the magnetic field. This limitation is not so restrictive as to render the system useless, though. With appropriate planning and orbit design, many useful applications of an LAO can be realized. Described in Sec. IV are methods for changing orbital energy, changing the orbit's angular momentum (both magnitude and direction), and arbitrary control of right ascension and

Presented as Paper 6804 at the AIAA Guidance, Navigation, and Control Conference, Keystone, CO, 20–23 August 2006; received 29 November 2006; revision received 20 June 2007; accepted for publication 5 July 2007.

*Graduate Research Assistant, Department of Mechanical and Aerospace Engineering, 245 Upson Hall.

†Assistant Professor, Department of Mechanical and Aerospace Engineering, 212 Upson Hall.

argument of perigee for certain situations. This control allows for the creation of certain new Earth-synchronous orbits.

II. Related Work and Concept Overview

The LAO builds on previous research in many fields. Some of this work is presented here. It offers insight into some of the design and implementation issues of LAO-capable spacecraft and guides our development of a candidate space-system architecture.

A. Related Work

The contribution of the Lorentz force to orbiting bodies has been observed in natural planetary systems. Schaffer and Burns [5,6] have analyzed the dynamics of dust particles charged by the plasma environment around Jupiter. They have shown that the motions of these small charged grains can be greatly affected by Lorentz mechanics. This mechanism can be used to explain sparse, latitudinally thick, rings found around Jupiter's main rings. Hamilton derives expressions for time-averaged perturbation equations of dust particles around Saturn [7], some of which are also derived here. Although the fundamental dynamics of these particles is well understood, we seek applications for controlled-charge spacecraft in a variety of orbits.

Just as dust grains naturally achieve some nonzero charge around Jupiter, a satellite orbiting in a plasma environment will attain a static charge. Many Earth-orbiting spacecraft, such as the SCATHA mission, have measured this effect [8]. Garrett and Whittlesey [9] present an overview of the natural charging that occurs in the Earth environment. Spacecraft in Earth orbit tend to naturally hold a negative charge, and this charging occurs with a small time constant (on the order of milliseconds) [10].

If a satellite is to control its charge, it must exchange charge with the plasma environment in some way. One solution involves the use of ion or electron beams. Charging a spacecraft with particle beams has been extensively studied in conjunction with research in both missile defense and ionospheric physics. An overview of beam effects on satellites can be found in Lai [11]. In fact, Hough [12] describes the trajectory perturbations on a ballistic missile due to Lorentz force. However, this work is the only study of the effect of the Lorentz force on a spacecraft's orbit that has been found by the authors. The LAO was first proposed by Peck [2].

Other studies have proposed various ways to use charged spacecraft and magnetic field interactions for many applications. King et al. [13] and Schaub [14] present the idea of coulomb spacecraft formations (CSF). Satellites in a CSF formation are electrostatically charged, and some measure of formation control is provided by the coulomb forces between the various satellites. The CSF system faces many of the same system architecture challenges as LAO. However, due to plasma shielding, a CSF is impractical in LEO, whereas an LAO is more effective in LEO, where the magnetic field strength is greater. In addition to tethered satellites, Bergamin et al. [15] propose propellantless electromagnetic propulsion via a current loop partially shielded by superconductive magnets. A further application of charged satellites in a magnetic field is given by Tikhonov [16]. He proposes the use of nonuniform charging on a satellite to control attitude via the Lorentz force. This idea faces many of the same challenges and dynamics as the LAO systems but are not considered further here. The scope of the present study extends only to orbit dynamics.

B. Issues and Complexities in LAO

A convenient and highly simplified model of an LAO consists of the geomagnetic field as a simple dipole, the magnetic north pole and the true north pole perfectly aligned, and the space environment as a true vacuum. Of course, these simplifications neglect certain subtleties. The Earth's magnetic field is nonuniform and varies in time; it is frequently described by a spherical-harmonic expansion. The solar wind causes large spatial and temporal deformations of the field [4]. In addition, magnetic north does not align with true north; magnetic north is about 10 deg south of the true pole. Furthermore, because the field rotates with the Earth, the relationship between the two poles is not constant in an inertial frame. The simpler nontilted-dipole model allows for clean, simple analytical results to be obtained. These simple results provide both insight into the problem and a starting point for a more in-depth analysis.

The Earth's plasma environment is also difficult to model, but plasma effects turn out to be critically important for the design of a practical LAO spacecraft. Plasma composition, temperature, and density vary both spatially and temporally over a large range of values in ways that are currently unpredictable. The interactions between a charged satellite and the plasma are also difficult to model and are affected by these subtleties. So predictions of the charge decay of a satellite are uncertain at best [4].

The scope of the present study does not include most of these complexities. Most cases here assume a nontilted-dipole geomagnetic field. The implementation of an LAO is only briefly discussed, and most of what follows assumes that a required charge on the satellite can be delivered, regardless of plasma environment or power constraints. This paper focuses on the basic orbital dynamics of an LAO and presents dynamically interesting cases with applications inspired by these results. We focus on these applications in the hope that they may motivate further work in the practical aspects of building an LAO-capable spacecraft.

C. Possible System Architecture

There appear to be many ways to achieve some level of charge on a spacecraft. The present study considers only the amount of charge, not how it is achieved. Any method that achieves a certain electrostatic charge on the satellite will bring about the same orbital dynamics. A possible system architecture is shown in Fig. 1. This system is somewhat reminiscent of a Van de Graaff generator [17]. A boom extending from one side of the satellite contains an electron gun. This electron gun interacts with the ambient plasma and expels a beam of electrons. The loss of electrons through the beam causes a net positive charge to build up on the satellite. A conductive sphere is placed around the main spacecraft bus to hold this charge.

The matter of how much charge can be held on a satellite is no mean problem, but it is not considered in depth here. In general, the best way to store charge on an LAO spacecraft is a system that maximizes the average distance between charged particles, and thus the potential associated with them, while minimizing the mass of the storage apparatus. Furthermore, exploiting the geometry of the plasma sheath structure that arises due to ionospheric interactions may provide significant additional capacitance over the vacuum case. The power required to combat incident plasma currents is not yet well understood, although power, rather than capacitance, will ultimately limit the achievable charge-to-mass ratio.

III. Equations of Motion

We derive equations of motion for LAOs. These equations can include far more detailed models of magnetic field orientations and representations, but doing so obscures the fundamental behaviors for

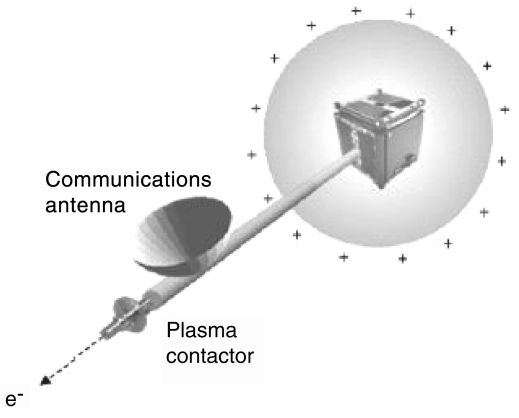

Fig. 1 Possible LAO system architecture.

a minimal improvement in precision. We deal first with the simplified case of a single charged satellite in a dipole field that is not tilted with respect to the axis of rotation of the planet. This result is followed by a more general treatment of energy and angular momentum changes due to the Lorentz force.

A. Equations of Motion in a Nontilted-Dipole Field

The relevant vectors are represented in an Earth-centered inertial spherical coordinate system. The spherical coordinates consist of radius r, colatitude angle ϕ, and azimuth from the x direction θ, as shown in Fig. 2. The magnetic field is expressed as

$$\mathbf{B} = \frac{B_0}{r^3}[2\cos\phi\hat{\mathbf{r}} + \sin\phi\hat{\boldsymbol{\phi}} + 0\hat{\boldsymbol{\theta}}] \tag{3}$$

where B_0 is the strength of the field in Wb · m. The field rotates with the Earth. In the nontilted field case, r and ϕ are equivalent in both the rotating field frame and the inertial frame. Because the dipole is axisymmetric, the magnetic azimuth does not directly contribute to the Lorentz force. For the Earth, the geographic North Pole is in fact the magnetic South Pole; the north side of a compass needle is attracted to the geomagnetic south pole. Because we desire a coordinate system that has geographic north in the z direction, we work with a dipole field that is essentially flipped upside down. We correct for this fact by using a B_0 term that is negative.

The acceleration in inertial coordinates is given by

$$\mathbf{a} = \mathbf{F}/m = -\frac{\mu}{r^3}\mathbf{r} + \frac{q}{m}(\mathbf{v} - \omega_E\hat{\mathbf{n}} \times \mathbf{r}) \times \mathbf{B} \tag{4}$$

where q/m is the charge-to-mass ratio of the satellite in C/kg, and $\hat{\mathbf{n}}$ is a unit vector in the direction of the true north pole.

Expressing the Lorentz force (per unit mass) in the spherical inertial frame yields

$$\mathbf{F}_L = \frac{q}{m}\frac{B_0}{r^3}\begin{bmatrix} -r\dot{\theta}\sin^2\phi + \omega_E r\sin^2\phi \\ 2r\dot{\theta}\sin\phi\cos\phi - 2\omega_E r\cos\phi\sin\phi \\ \dot{r}\sin\phi - 2r\dot{\phi}\cos\phi \end{bmatrix} \tag{5}$$

Combining the Lorentz term with gravity and the standard accelerations in spherical coordinates gives the following three equations of motion:

$$\ddot{r} = r\dot{\theta}^2\sin^2\phi + r\dot{\phi}^2 - \frac{\mu}{r^2} - \frac{q}{m}\frac{B_0}{r^3}[r\dot{\theta}\sin^2\phi - \omega_E r\sin^2\phi] \tag{6}$$

$$r\ddot{\phi} = -2\dot{r}\dot{\phi} + r\dot{\theta}^2\sin\phi\cos\phi + \frac{q}{m}\frac{B_0}{r^3}2[r\dot{\theta}\sin\phi\cos\phi - \omega_E r\cos\phi\sin\phi] \tag{7}$$

$$r\ddot{\theta}\sin\phi = -2\dot{r}\dot{\theta}\sin\phi - 2r\dot{\phi}\dot{\theta}\cos\phi + \frac{q}{m}\frac{B_0}{r^3}[\dot{r}\sin\phi - 2r\dot{\phi}\cos\phi] \tag{8}$$

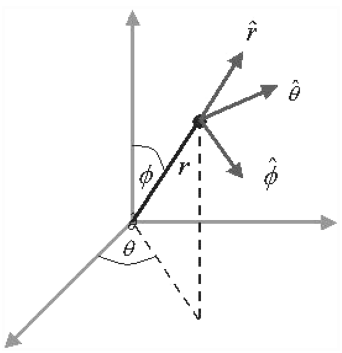

Fig. 2 Spherical coordinates used in the derivation of the equations of motion.

Equations (6–8) represent a sixth-order system that describes the motion of any orbit of a charged satellite in a nontilted-dipole magnetic field.

B. General Energy and Angular Momentum Change

General time rates of change of energy and angular momentum due to the Lorentz force are derived. With these derivatives, the time rates of change of various orbital elements can be found following the method of Burns [18]. The work-energy principle states

$$\dot{E} = \mathbf{v} \cdot \mathbf{F} \tag{9}$$

where E is the total energy of the system per unit mass, $\mathbf{F}$ is the applied force per unit mass, and $\mathbf{v}$ is the body's velocity. Including the Lorentz force gives

$$\dot{E} = \frac{q}{m}\mathbf{v} \cdot [\mathbf{B} \times (\omega_E\hat{\mathbf{n}} \times \mathbf{r})] \tag{10}$$

Equation (10) shows that only the rotation of the magnetic field allows the Lorentz force to do work on the satellite. A general magnetic force is conservative; thus the change in energy comes not from the magnetic field, but indirectly from the rotation of the Earth. Equivalently, a moving magnetic field is associated with an electric field, and this induced electric field can do work on a satellite.

Applying the triple-cross-product identity to Eq. (10) yields

$$\dot{E} = \frac{q}{m}\omega_E[(\mathbf{v} \cdot \hat{\mathbf{n}})(\mathbf{B} \cdot \mathbf{r}) - (\mathbf{v} \cdot \mathbf{r})(\hat{\mathbf{n}} \cdot \mathbf{B})] \tag{11}$$

Equation (11) is general. It describes any orbit or magnetic field configuration.

Change in orbital angular momentum arises from the torques applied to the system by the Lorentz force, or

$$\dot{\mathbf{h}} = \mathbf{r} \times \mathbf{F}_L \tag{12}$$

where $\mathbf{h}$ is the angular momentum per unit mass of the system. Substituting for $\mathbf{F}_L$ and simplifying gives

$$\dot{\mathbf{h}} = \frac{q}{m}[(\mathbf{B} \cdot \mathbf{r})\mathbf{v} - (\mathbf{r} \cdot \mathbf{v})\mathbf{B} - \omega_E(\mathbf{B} \cdot \mathbf{r})(\hat{\mathbf{n}} \times \mathbf{r})] \tag{13}$$

Depending on the orbital and magnetic configurations, we may change both the magnitude and direction of the angular momentum vector. Changing the direction of this vector allows some measure of control over both the inclination and right-ascension angles of the orbit. This control is examined in more detail for two cases in Sec. IV.

IV. Applications

Using the Lorentz force to achieve a mission objective is sometimes not an intuitive exercise. A charged spacecraft cannot control the direction of the force, only magnitude and perhaps the sign, depending on the implemented architecture. The force is also perpendicular to the field-fixed velocity of the spacecraft. Were the magnetic field not rotating, no energy could be added to an LAO; but with the rotating field, the energy and angular momentum of the orbit can be changed in most cases. Also, with appropriate control of the charge on the satellite, controlling energy and momentum allows for regulation of most of the orbital elements of the spacecraft. Two specific cases are developed here: the polar circular orbit and the general equatorial orbit, both in a nontilted-dipole field. Additionally, the Earth's oblateness effects are examined.

A. Polar Circular Orbit in a Nontilted-Dipole Field

We apply the general energy and momentum relationships in Eqs. (11) and (13) to two specific cases to develop some simple and interesting results.

1. *Analytical Results*

First we examine a polar circular orbit in a nontilted-dipole magnetic field. In this case, Eq. (11) becomes

$$\dot{E} = 2\frac{q}{m}\omega_E B_0 \sqrt{\mu} r^{-5/2} \sin u \cos u \tag{14}$$

where r is the radius of the orbit, and u is the argument of latitude of the satellite. The argument of latitude is the angular position of the satellite around the orbit measured from the right ascension of the vehicle in the equatorial plane. The expression in Eq. (14) is an odd periodic function and thus contributes no secular change to the energy of the orbit. However, the radius of the orbit oscillates with a frequency of twice per orbit. Expressing the radius of the circular orbit as a function of energy, and using Eq. (14), gives an expression for the time rate of change of the radius of the orbit:

$$\dot{r} = 4\frac{q}{m}\omega_E \frac{B_0}{\sqrt{\mu}} r^{-1/2} \sin u \cos u \tag{15}$$

For constant q/m, Eq. (15) is periodic over an orbit. The radial velocity (and thus eccentricity) remains small for a constant q/m, keeping the assumptions of a Keplerian polar circular orbit valid. The simulation results shown in Sec. IV.A.2 back up this assumption, showing that deviations in eccentricity and inclination remain small. However, if we choose to control the charge as a function of the argument of latitude, a secular change in the radius (and eccentricity) of the orbit can be obtained.

Similarly, the angular momentum rate of a circular polar LAO is examined with Eq. (13), with an orthogonal coordinate system having the x direction along the line of nodes, the y direction aligned with the north pole, and the z direction necessarily along the orbit's angular momentum vector. With this coordinate system, the properties of a polar circular orbit, and Eq. (13), the vector derivative of angular momentum becomes

$$\dot{\mathbf{h}} = 2\frac{q}{m}\frac{B_0}{r^2}\begin{bmatrix} -v_c \sin^2 u \\ v_c \sin u \cos u \\ r\omega_E \sin u \cos u \end{bmatrix} \tag{16}$$

Equation (16) represents the time rate of change of the angular momentum vector due to the Lorentz force for a circular polar LAO.

We use the vector derivative in Eq. (16) to define several scalar derivatives of interest, including the time rates of change of the inclination angle, the right-ascension angle, and the magnitude of the angular momentum. First, the derivative of the scalar angular momentum magnitude is given by

$$\dot{h} = 2\frac{q}{m}\frac{B_0}{r}\omega_E \sin u \cos u \tag{17}$$

Thus, the magnitude of the angular momentum vector changes in a purely periodic manner under a constant charge.

The inclination angle i is defined in terms of the angular momentum vector $\mathbf{h}$ by

$$\hat{\mathbf{n}} \cdot \mathbf{h} = h \cos i \tag{18}$$

Differentiating Eq. (18) to find the time rate of change of i gives

$$\frac{\mathrm{d}i}{\mathrm{d}t} = \frac{-2(q/m)(B_0/r^2)\sin u \cos u[v_c - r\omega_E \cos i]}{r v_c \sin i} \tag{19}$$

where the notation $\mathrm{d}i/\mathrm{d}t$ is used for clarity. Again, for constant charge, Eq. (19) is nonsecular, oscillating at a frequency of twice per orbit.

Using the results of Burns [18], Eq. (16) is used to find the time rate of change of right ascension of the ascending node. Recognizing that in a circular polar orbit, the circular velocity v_c can be replaced by $r\dot{u}$, the derivative of right ascension is

$$\dot{\Omega} = -2\frac{q}{m}\frac{B_0}{r^2}\sqrt{\frac{r}{\mu}}\sin^2 u \dot{u} \tag{20}$$

Equation (20) is an even secular function. The ascension of the orbit changes over the course of one orbit.

We can determine an average change in right ascension per orbit by integrating Eq. (20) around one complete orbit. The change in right ascension per orbit ($\Delta\Omega$) is given by

$$\Delta\Omega = -2\pi\frac{q}{m}\frac{B_0}{r^2}\sqrt{\frac{r}{\mu}} \tag{21}$$

Thus, for the circular polar orbit in a nontilted-dipole case, we can set an arbitrary change in right ascension per orbit. Defining the average time derivative of right ascension as $\dot{\Omega}_{\mathrm{avg}}$, equal to Eq. (21) divided by the orbital period, and inverting the result gives the following simple relationship between the charge-to-mass ratio q/m and the average right-ascension rate $\dot{\Omega}_{\mathrm{avg}}$, circular-orbit radius r, and magnetic field strength B_0:

$$\frac{q}{m} = -\frac{\dot{\Omega}_{\mathrm{avg}} r^3}{B_0} \tag{22}$$

We can now calculate the necessary charge-to-mass ratio for any desired right-ascension rate.

Changing the right ascension of a polar orbit essentially amounts to changing longitude on the groundtrack of the satellite (see Fig. 3). Arbitrary right-ascension control can greatly increase the efficiency of a polar LEO imaging satellite. If full charge control is possible (both positive and negative charges), then the satellite can acquire a target faster and can stay in the neighborhood of the target longer. In fact, if an average right-ascension rate equal to the rate of the Earth's rotation is acquired, then a satellite can have a single-orbit repeat groundtrack. The satellite would pass over exactly the same points on the Earth during every orbit. Thus, the orbit becomes a LEO GT-1 orbit. This groundtrack would allow a satellite to pass over an imaging target every 90 min rather than, at most, twice a day for an uncontrolled LEO polar satellite.

Solving for the required charge-to-mass ratio for an LAO GT-1 yields

$$\left(\frac{q}{m}\right)_{\mathrm{GT\text{-}1}} = -\frac{\omega_E r^3}{B_0} \tag{23}$$

When evaluated for a circular orbit with 400-km altitude, Eq. (23) reveals that a q/m of 2.831 C/kg is required for geosynchronous behavior.

Another possible application is a sun-synchronous LEO polar orbit at any altitude. The sun-synchronous condition is a right-ascension rate of $\dot{\Omega}_{\mathrm{ss}} = 2\pi$ rad/year. This rate yields a charge-to-mass ratio for maintaining a sun-synchronous orbit of

$$\left(\frac{q}{m}\right)_{\mathrm{ss}} = -\frac{\dot{\Omega}_{\mathrm{ss}} r^3}{B_0} \tag{24}$$

For example, a 400-km orbit requires a ratio 0.0078 C/kg for sun synchronicity.

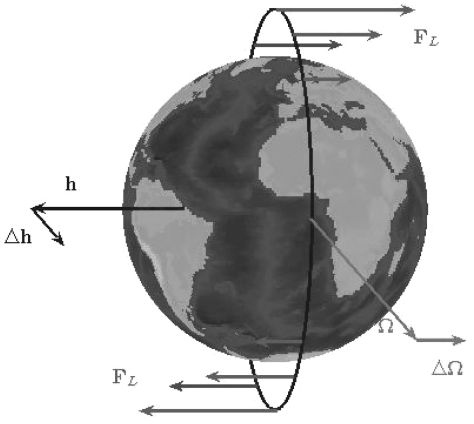

Fig. 3 Graphical representation of the vectors involved in an LAO GT-1 orbit.

Table 1 Physical parameters common to all simulations

Parameter	Value
ω_E	7.272*e*-5 rad/s
μ	3.986*e*14 m^3/s^2
B_0	−8.000*e*15 Wb · m

Table 2 Initial conditions for polar circular orbit

Property	Value
Altitude	400 km
q/m	2.831 C/kg
Integration time	5 orbits

The nonperiodic change in right ascension persists for orbits that are not necessarily polar or circular. By extending the process used to derive the polar case to a general orbit (still assuming a nontilted-dipole field), an expression analogous to Eq. (22) is found for a general orbit:

$$\frac{q}{m} = \frac{\dot{\Omega}_{\text{avg}} a^3}{B_0}(1-e^2)^{3/2} \times \frac{1}{\omega_E \sqrt{a^3/\mu}(1-e^2)^2 \cos i \frac{e^2-[(1-e^2)^{1/2}-1]^2 \cos 2\omega}{e^2} - 1} \tag{25}$$

Equation (25) is valid for any elliptical orbit under the influence of a nontilted-dipole.

2. *Numerical Simulation*

A numerical simulation is developed to test several of the previous analytical results. The simulation is a Runge–Kutta integration of the sixth-order system defined by Eqs. (6–8), performed by Matlab. The simulation is valid for any orbit for a charged satellite in a nontilted-dipole field. Table 1 shows the set of physical parameters common to all simulations.

The polar circular orbit is integrated from the initial conditions in Table 2. The charge-to-mass ratio of 2.831 is chosen based on Eq. (23). Figure 4 shows the resulting orbital path. This path is plotted in a frame that rotates with the Earth, to highlight the GT-1 nature of the orbit. The orbit is shown to scale with the image of the Earth. Figure 4 shows a slight deviation from a perfect GT-1 orbit. This discrepancy is explained by Fig. 5. This figure compares the forces acting on the satellite over one orbital period. The magnitudes of both gravity and the Lorentz force are shown. In this GT-1 polar scenario, the Lorentz force is quite significant with respect to gravity, which causes large orbital element changes, violating the osculating-element assumption. A large Lorentz force causes the orbital eccentricity to be nonzero, creates wobbles in the inclination, and keeps the orbital speed from being constant. These perturbations on the orbit cause slight inaccuracies in the expressions derived in Sec. IV.A.1 related to a polar circular orbit.

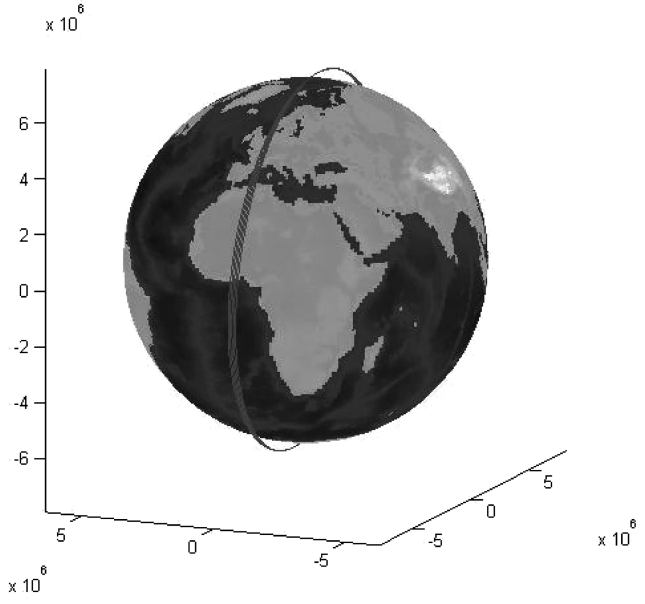

Fig. 4 Track of a GT-1 LAO orbit in a frame rotating with Earth with $q/m = 2.83$ C/kg.

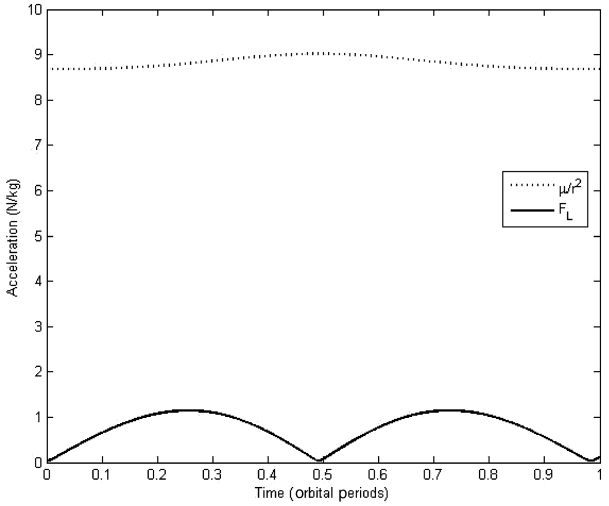

Fig. 5 Comparison of gravitational and Lorentz acceleration magnitudes for a GT-1 LAO orbit with $q/m = 2.83$ C/kg.

However, the small difference in calculated and desired right-ascension angles is due only to wind up of small errors in the predicted right-ascension rate over time. The top plot of Fig. 6 shows both the numerically calculated and the analytically derived right-ascension-angle rates. The analytical results are based on the expression in Eq. (20); the numerical result is based upon changes in the angular momentum vector of the orbit determined from the state of the system at any given time. As expected, the right-ascension rate is zero as the satellite crosses the equator, and it is large and positive as it crosses the poles. The average values of the curves in Fig. 6 are

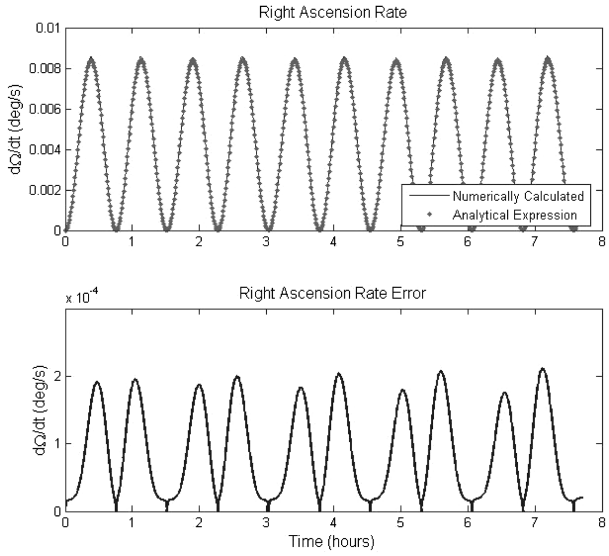

Fig. 6 Time rate of change in right ascension for a GT-1 LAO orbit with $q/m = 2.83$ C/kg. The top plot shows both analytical and numerical calculations of the right ascension. The bottom plot shows the error between these two curves.

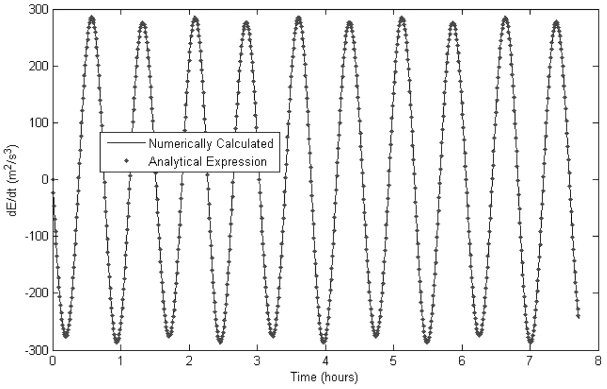

Fig. 7 Time rate of change of orbital energy for a GT-1 LAO orbit with $q/m = 2.83$ C/kg.

greater than zero, causing a secular increase in the right ascension of the orbit. These two curves match almost exactly, with small, but persistent, errors. The rate error is shown in the bottom plot of Fig. 6. The size of the errors is an order of magnitude smaller than the rates. In practice, closed-loop control of the charge might be used to trim the errors that arise due to unmodeled dynamics in the open-loop system. The closed-loop case is addressed later in Sec. V.C.

Finally, Fig. 7 shows the time rate of change of orbital energy throughout the simulation. The solid line represents the numerically calculated energy rate based on the state vector at each time, and the dotted line represents the derived expression shown in Eq. (14). These two curves match closely. However, the energy rate is centered around zero, and thus there is no secular change in the orbital energy.

B. Equatorial Orbit in a Nontilted-Dipole Field

A second simple case to consider is an equatorial orbit in a nontilted-dipole field. The true equator and the magnetic equator are aligned in this situation, and the magnetic field is perpendicular to these planes. The eccentricity can be nonzero in this case.

1. *Analytical Results*

In the equatorial eccentric-orbit case, Eq. (11) becomes

$$\dot{E} = \frac{q}{m}\omega_E B_0 \sqrt{\mu}[a(1-e^2)]^{-5/2} e \sin\nu(1+e\cos\nu)^2 \tag{26}$$

where a is the orbit semimajor axis, e is the orbital eccentricity, and ν is the true anomaly. Note the dependence on the eccentricity e. The Lorentz force cannot add energy to a circular equatorial orbit. Equation (26) leads to a time rate of change of the semimajor axis of

$$\dot{a} = 2\frac{q}{m} e a^2 \omega_E \frac{B_0}{\sqrt{\mu}}[a(1-e^2)]^{-5/2}\sin\nu(1+e\cos\nu)^2 \tag{27}$$

Again, the rate in Eq. (27) is nonsecular, but with proper modulation of q/m, the size of the equatorial orbit can be controlled using the Lorentz force.

Using the specifics of an equatorial orbit in Eq. (13) gives a time rate of change of vector angular momentum of

$$\dot{\mathbf{h}} = -\frac{q}{m}(\mathbf{r}\cdot\mathbf{v})\frac{B_0}{r^3}\hat{\mathbf{h}} \tag{28}$$

where $\hat{\mathbf{h}}$ is a unit vector in the $\mathbf{h}$ direction. Because the rate in Eq. (28) only has a component in the direction of $\mathbf{h}$, it represents only a change in the scalar magnitude of $\mathbf{h}$. This scalar momentum change is expressed as

$$\dot{h} = \frac{q}{m} B_0 \sqrt{\mu}[a(1-e^2)]^{-5/2} e \sin\nu(1+e\cos\nu)^2 \tag{29}$$

which is another periodic function with no secular terms. Here, the direction of h cannot be controlled, which means the inclination and right-ascension angles cannot be changed.

Following Burns [18] and using Eqs. (26) and (29), an expression for the time rate of change of orbital eccentricity under the Lorentz force in a equatorial orbit is

$$\dot{e} = -\frac{q}{m} B_0 \frac{\sin\nu(1+e\cos\nu)^2}{[a(1-e^2)]^{3/2}}\left[\frac{1}{a^{3/2}(1-e^2)^{1/2}} - \frac{\omega_E}{\sqrt{\mu}}\right] \tag{30}$$

which is periodic in true anomaly. If one starts with an initially circular orbit, the eccentricity of the orbit should be changed to facilitate the control of energy.

Also from Burns [18], we develop an expression for the argument of perigee rate using Eqs. (26) and (29). Simplification gives

$$\dot{\omega} = \frac{(q/m)B_0}{\sqrt{\mu}}\left[\frac{2}{[a(1-e^2)]^{3/2}} + \frac{2e\cos\nu}{[a(1-e^2)]^{3/2}} + \frac{\cos\nu}{a^{3/2}e(1-e^2)^{1/2}} - \frac{\omega_E\cos\nu}{e\sqrt{\mu}}\right]\dot{\nu} \tag{31}$$

where the standard time rate of change of true anomaly for a Keplerian orbit was used. The first term in brackets in Eq. (31) gives rise to a secular change in the argument of perigee for a constant charge-to-mass ratio. This secular perigee change has many interesting, if somewhat esoteric, applications. Perigee control allows for the cancellation of various natural perturbations on the argument of perigee, such as J_2 effects and lunar and solar tides. Another use may be to create a Molniya-type orbit at zero inclination (and, most likely, other inclinations). Building on the same ideas as the GT-1 LAO orbits discussed previously, perigee control also allows for matching the Earth's rotation rate. The line of apsides of such a synchronous orbit would remain at a constant longitude on Earth's surface. Thus, LAO creates possibilities for other kinds of synchronous orbits, rather than just GT-x orbits.

To evaluate this concept of precessing the line of apsides, we seek an expression for the q/m necessary to generate a certain average perigee rate. Integrating Eq. (31) around one orbit gives an expression for change in the argument of perigee per orbit $\Delta\omega$:

$$\Delta\omega = \frac{4\pi(q/m)B_0}{\sqrt{\mu}[a(1-e^2)]^{3/2}} \tag{32}$$

For a certain desired rate of change in the argument of perigee $\dot{\omega}_{\text{des}}$, we require that $\Delta\omega/\Delta t = \dot{\omega}_{\text{des}}$, where we set Δt to be one orbital period. Setting the resulting expression for $\Delta\omega$ equal to Eq. (32) and solving for q/m gives a required charge-to-mass ratio for some desired rate of perigee change:

$$\frac{q}{m} = \frac{\dot{\omega}_{\text{des}} a^3(1-e^2)^{3/2}}{2B_0} \tag{33}$$

Equation (33) has similar dependencies as Eq. (22), the charge-to-mass ratio required for a particular right-ascension rate for a polar circle. However, in the equatorial case, the eccentricity plays an important role in the magnitude of charge required. A higher eccentricity corresponds to a higher velocity at perigee for a given orbit size, which makes a more effective use of the Lorentz force, allowing for a smaller charge-to-mass ratio. Equation (33) applies for any desired rate of change for argument of perigee, including mitigating oblateness and third-body effects, as well as introducing synchronous behavior. However, larger rates introduce inaccuracy in the q/m predicted by this osculating-elements approach. The derivation of Eq. (33) assumes that all the other orbital elements are changing slowly or are not explicit functions of ν, and this may not be the case with a large charge-to-mass ratio.

The secular change in the argument of perigee under a constant charge also arises in nonequatorial orbits. Following the same method as for the equatorial case, but generalized for any elliptical orbit, yields an expression for the charge-to-mass ratio required for a desired perigee rate:

$$\frac{q}{m} = \frac{\dot{\omega}_{\text{des}} a^3 (1-e^2)^{3/2}}{B_0 \cos i} \times \left[3 - \omega_E \sqrt{\frac{a^3}{\mu}} (1-e^2)^2 \cos i \frac{e^2 - [(1-e^2)^{1/2} - 1]^2 \cos 2\omega}{e^2} \right]^{-1} \tag{34}$$

A subtlety in the derivation of Eq. (34) arises from the coupled changes in right ascension and argument of perigee in an inclined orbit, hence the similarities between Eqs. (25) and (34).

Equation (34) gives the time rate of change of perigee relative to an inertial coordinate system. This rate is the superposition of two different rates: the rate of change of argument of perigee within the orbit plane, and the change in perigee due to the fact that the right ascension, and thus orbital plane itself, is changing. To create the ω-synchronous orbit, the rate of in-plane perigee change must be equal to the rotation rate of the Earth. Subtracting the rates due to right-ascension rate of change gives

$$\frac{q}{m} = \frac{\omega_E a^3 (1-e^2)^{3/2}}{2B_0 \cos i} \tag{35}$$

which differs only by a factor of $1/\cos i$ from Eq. (33). Again, Eq. (35) is only valid for situations in which the desired rate of perigee change is based on a relationship with the rotating Earth, rather than some absolute inertial rate.

2. *Numerical Simulation*

The equatorial, eccentric, constant-charge simulation is initialized with the values shown in Table 3, using the same model as in the case of the polar orbit. The chosen value of q/m is designed to produce an Earth-synchronous motion of the perigee of the orbit. The value is calculated from Eq. (33), with a desired rotation rate designed to match the Earth's rotation, or $\dot{\omega}_{\text{des}} = \omega_E$.

Figure 8 shows the orbital path of the satellite over one day. Again, the orbit is to scale with the depiction of the Earth as viewed from above the north pole. The orbital path is shown in a coordinate system rotating with the Earth.

The rotating frame view in Fig. 8 shows that the charge-to-mass ratio used in the simulation was not large enough to perfectly cancel the Earth's rotation with perigee motion. If the correct charge were used, the rotating frame view would show only a single curve. The top plot of Fig. 9 shows the numerically calculated and analytically derived arguments of perigee for this case. The numerical values are represented by the solid line. The dotted line represents the analytical values, calculated by numerically integrating Eq. (31). Although these two curves match quite precisely, we see that the perigee angle does not reach 360 deg after one day as intended. Figure 9 gives confidence in the result for time rate of change of perigee expressed in Eq. (31), but shows that accuracy is lost in integrating this data to obtain Eq. (33). The perigee error, the difference between the numerical and analytical curves, is shown in the bottom plot of Fig. 9. The error is significantly smaller than the perigee values. In the integration of Eq. (31), we assumed that the semimajor axis and eccentricity were changing slowly enough to be independent of true anomaly. The charge-to-mass ratios are large enough in this case to make that a poor assumption. However, for a smaller desired perigee rate, like mitigating J_2 effects, Eq. (33) is quite accurate. Creating the

Table 3 Initial conditions for equatorial constant-charge integration

Property	Value
Perigee altitude	400 km
Apogee altitude	1500 km
Eccentricity	0.075
Semimajor axis	7328 km
q/m	−1.774 C/kg
Integration time	1 day

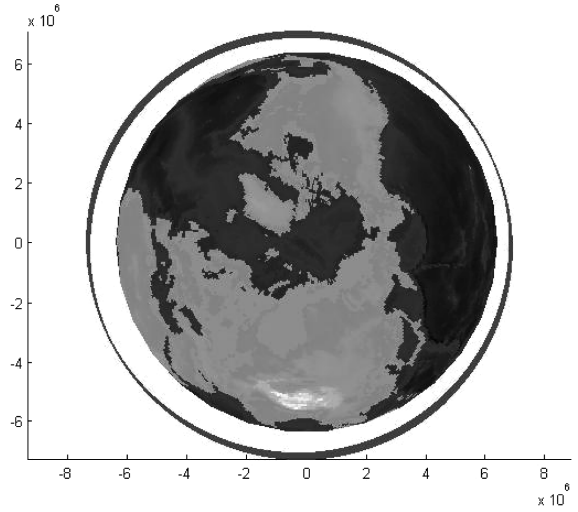

Fig. 8 Earth-fixed orbital path of an equatorial constant-charge LAO satellite with $q/m = -1.77$ C/kg, calculated for synchronous perigee movement.

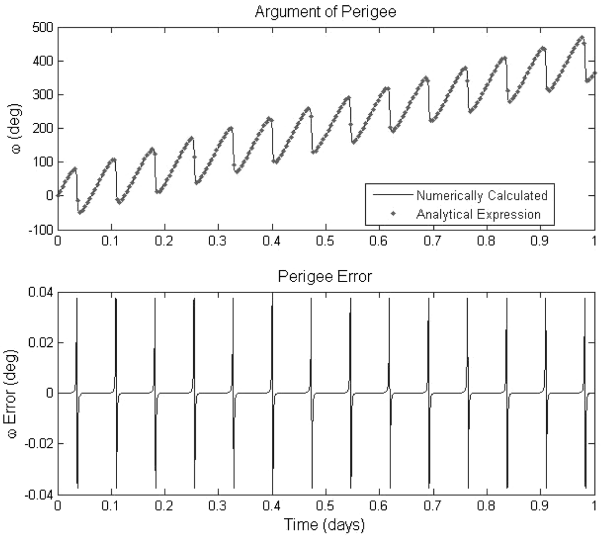

Fig. 9 Argument of perigee angle of an equatorial constant-charge LAO satellite with $q/m = -1.77$ C/kg. The top plot shows both analytical and numerical calculations of the argument of perigee. The bottom plot shows the error between these two curves.

Earth-synchronous effect is certainly possible, it just requires a larger q/m than predicted. Creating a closed-loop control system to adjust q/m can account for this variation, in addition to correcting for imperfections in the magnetic field model, plasma variations, etc. Equation (33) represents a starting point for system design and closed-loop control.

The results demonstrate that a constant-charge equatorial LAO satellite can have an arbitrary time rate of change of argument of perigee. The required charge-to-mass ratio for a desired rate depends solely on the initial orbit configuration and the magnitude of the desired change. The orbital energy and eccentricity also change in a predictable manner, but with no secular variations.

The simulations, both in this section and in Sec. IV.A.2, have shown excellent agreement between the derived equations of motion and the analytical expressions for the orbital changes in a Lorentz-augmented orbit. We see that useful and desirable changes can be made to orbits using this system. Although only simulations of polar and equatorial orbits are presented here, an arbitrarily inclined orbit will just combine the properties of these two results in some way. Furthermore, the approximation of osculating elements yields convenient expressions that provide insight into the behaviors for

only small inaccuracy. Only constant charges are examined here. Simple charge controls can be applied to produce secular changes in any of the perturbations equations derived previously. Atchison et al. [19] provide a closer examination of the nonconstant-charge case.

C. Mitigation of the Earth's Oblateness Effects

The nonsphericity of the Earth causes secular changes in both the right ascension and argument of perigee of a spacecraft, herein referred to as J_2 effects [1]. The generally accepted secular time rates of change due to J_2 are

$$\dot{\Omega}_{J2} = -\frac{3}{2}\frac{J_2 R_E^2 \sqrt{\mu}}{a^{7/2}}\frac{\cos i}{(1-e^2)^2} \tag{36}$$

$$\dot{\omega}_{J2} = \frac{3}{4}\frac{J_2 R_E^2 \sqrt{\mu}}{a^{7/2}}\frac{4-5\sin^2 i}{(1-e^2)^2} \tag{37}$$

It is trivial to use LAO to cancel the effect of J_2 on either the right-ascension angle or the argument of perigee. The rate calculated with Eq. (36) or Eq. (37) can simply be substituted into Eq. (25) or Eq. (34), respectively. For example, in an equatorial orbit with perigee at 400-km altitude and apogee at 1500 km, J_2 causes the argument of perigee to change by about 12.4 deg /day. The charge-to-mass ratio required to overcome this perturbation is about 0.042 C/kg.

There are orbits in which a constant-charge LAO can cancel the secular changes in both Ω and ω. These orbits can only exist below the J_2 critical angle of $i \approx 63.4$ deg or above the critical solution of $i \approx 116.6$ deg . Additionally, the effect of the Lorentz force must be equivalent to the J_2 effects in both the right ascension and the argument of perigee. This condition is true when the orbit in question satisfies the following expression:

$$\frac{3-K}{1-K} = \frac{4-5\sin^2 i}{2\cos^2 i} \tag{38}$$

where K is given by

$$K = \omega_E \sqrt{\frac{a^3}{\mu}}(1-e^2)^2 \cos i \frac{e^2 - [(1-e^2)^{1/2}-1]^2 \cos 2\omega}{e^2} \tag{39}$$

Although Eq. (38) does not easily yield simple relationships among the orbital elements, a minimum semimajor axis for this condition can be found. Under the most optimistic assumptions (namely, $e = 0$), the expression in Eq. (38) can be satisfied only if the polynomial

$$3\frac{w_E}{n}\cos^3 i + \cos^2 i - \frac{w_E}{n}\cos i + 1 = 0 \tag{40}$$

where n is the mean motion, has a valid solution. These solutions exist only when $w_E/n > 1$. Thus, the semimajor axis must exceed GEO altitude to fully cancel J_2 effects with a constant charge. At these altitudes, the J_2 and LAO effects would generally not be the dominant perturbative forces on the satellite.

V. Effects of a Tilted-Dipole Magnetic Field

The preceding analysis assumes the geomagnetic field to be a dipole for which the magnetic north pole is aligned with the Earth's geographic north pole. Although this assumption allows for several clean analytical results to be calculated, a more accurate model of the geomagnetic field is a dipole field for which the north pole axis is tilted with respect to true north. The actual geomagnetic north pole lies in northern Canada, tilted roughly 10 deg from geographic north.

A. Tilted Dipole and GT-1 Behavior

The tilted-dipole model is implemented with two new parameters: α represents the angle between the magnetic north pole and geographic north pole, and Ω_m represents the longitude of the magnetic north as measured from the inertial x axis. Because the geomagnetic field is locked in step with the Earth's rotation, Ω_m varies with respect to time as $\omega_E t + \Omega_m(0)$. The same general perturbation procedure as in Sec. IV is applicable to the tilted-dipole case. Applying the vector model of a dipole field, $\mathbf{B} = (B_0/r^3)[3(\hat{\mathbf{N}}\cdot\hat{\mathbf{r}})\hat{\mathbf{r}} - \hat{\mathbf{N}}]$, where $\hat{\mathbf{N}}$ is a unit vector along the magnetic north pole, to the general energy-rate equation (11) yields a new energy-rate relationship based on a tilted dipole:

$$\begin{aligned}\dot{E} = {} & \frac{q}{m}\omega_E B_0 \sqrt{\mu}\frac{[1+e\cos(u-\omega)]^2}{[a(1-e^2)]^{5/2}} \\ & \times \langle 2\sin i(\cos u + e\cos\omega)\{\cos(\Omega_m-\Omega)\sin\alpha\cos u \\ & + \sin(\Omega_m-\Omega)\cos i\sin\alpha\sin u + \sin i\cos\alpha\sin u\} \\ & - e\sin(u-\omega)[3\sin u\sin i\{\cos(\Omega_m-\Omega)\sin\alpha\cos u \\ & + \sin(\Omega_m-\Omega)\cos i\sin\alpha\sin u + \sin i\cos\alpha\sin u\} - \cos\alpha]\rangle\end{aligned} \tag{41}$$

Equation (41) is for a general elliptical orbit in a dipole field with any tilt. Equation (41) includes the nontilted-dipole case and encompasses the expressions in Eqs. (14) and (26). A similar expression can be derived for the angular momentum rate, which is not presented here for the sake of brevity. However, this angular momentum expression can be used to derive a relationship for the time rate of change of right-ascension angle under a tilted-dipole field, given by

$$\begin{aligned}\dot{\Omega} = {} & \frac{q}{m}\frac{B_0}{\sin i}\frac{[1+e\cos(u-\omega)]^2}{[a(1-e^2)]^3}\Big\{\cos\phi_m[-2\sin u - 2e\sin\omega \\ & - 3e\sin(u-\omega)\cos u] + e\sin(u-\omega)[\sin\alpha\cos(\Omega_m-\Omega)] \\ & - \frac{2\omega_E}{\sqrt{\mu}}\frac{[a(1-e^2)]^{3/2}}{[1+e\cos(u-\omega)]}\cos\phi_m\cos i\sin u\Big\}\end{aligned} \tag{42}$$

where ϕ_m is the satellite's magnetic colatitude:

$$\begin{aligned}\cos\phi_m = {} & \cos(\Omega_m-\Omega)\sin\alpha\cos u \\ & + \sin(\Omega_m-\Omega)\cos i\sin\alpha\sin u + \sin i\cos\alpha\sin u\end{aligned} \tag{43}$$

The effects of adding a tilt angle to the dipole field are numerically simulated based on a generalization of the nontilted-dipole integrations. The results of two simulations comparing the nontilted dipole and the tilted dipole are shown in Fig. 10. This figure shows two integrations, both beginning with same initial conditions: namely, a 400-km-alt polar circle with a charge-to-mass ratio calculated to give GT-1 behavior. The results are plotted in an Earth-fixed coordinate system. The left plot shows the integration in a nontilted dipole, giving the familiar GT-1 orbit. The right plot displays the result of a simulation including a dipole field tilted at an angle of 10 deg. This orbit is quickly driven away from GT-1 behavior. Each simulation lasts for a period of one day.

The cause of this deviation is found in the terms in Eq. (41) arising from the tilted dipole. In particular, the term of the form

$$\dot{E} \propto \cos(\Omega_m-\Omega)\sin\alpha\sin i\cos^2 u \tag{44}$$

causes a secular drift in the energy of the orbit away from its initial value. Initially, the quantity $\cos(\Omega')$ is constant, where Ω' is defined as the quantity $\Omega_m - \Omega$, because this condition embodies the LAO GT-1 behavior. A term similar to Eq. (44) also arises in the rate of angular momentum expression. Thus, E and $\mathbf{h}$ drift away from their nominal values, causing the spacecraft charge-to-mass ratio to be unsuitable for GT-1 behavior. As the orbit moves away from the GT-1 behavior, Ω' is no longer constant, and the spacecraft settles into a periodic motion that does not resemble GT-1.

The expression in Eq. (44) should go to zero when $\Omega' = \pm 90$ deg. Figure 11 shows numerical simulations for both of these initial orbit longitudes. The two plots in Fig. 11 represent the orbital energy of the

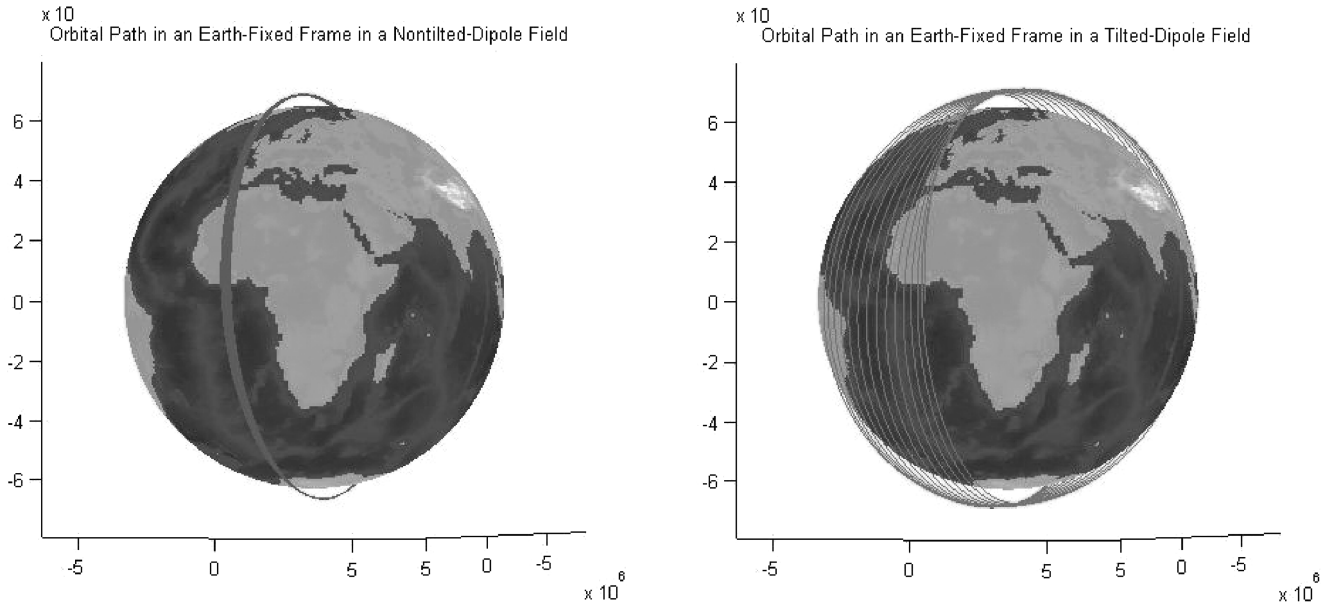

Fig. 10 Comparison between two integrations with the same initial conditions. The left plot uses a nontilted-dipole field; the right plot used a dipole field titled to 10 deg.

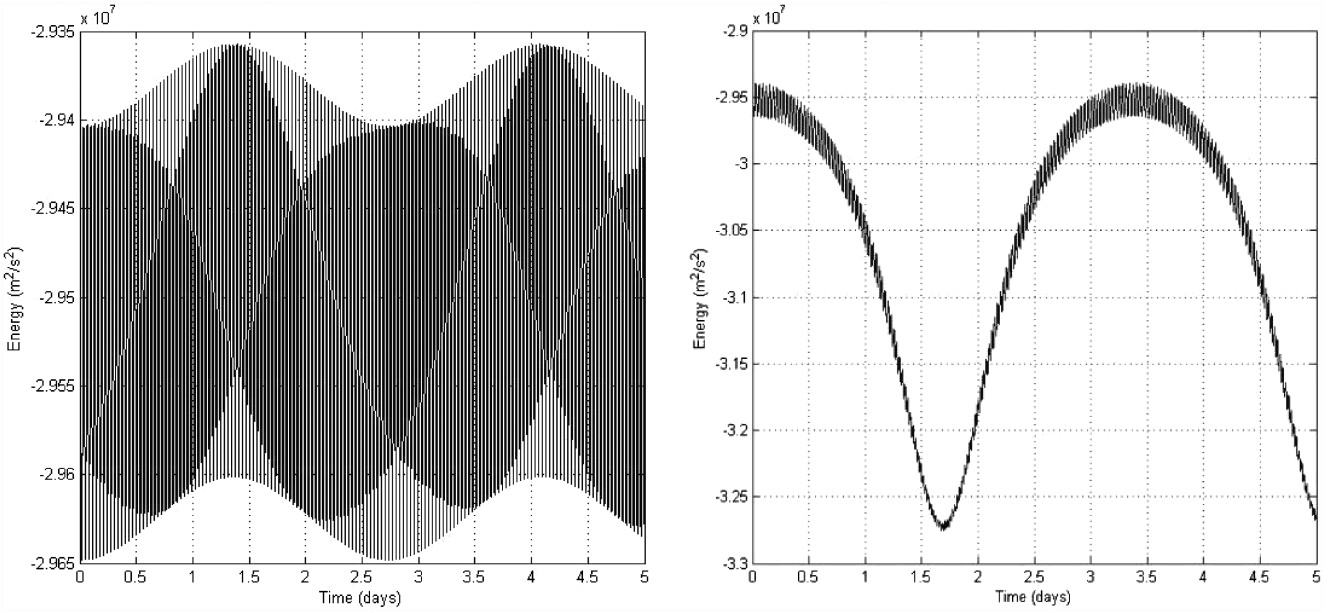

Fig. 11 The orbital energy of two tilted-dipole integrations with $q/m = -1.77$ C/kg, set to give GT-1 behavior. The left plot is for $\Omega' = -90$ deg. The right plot shows an initial angle of $\Omega' = +90$ deg.

spacecraft throughout the simulation. The left plot shows $\Omega' = -90$ deg, and the right displays $\Omega' = \pm 90$ deg. In the -90- deg case, the orbital energy remains nearly constant, and the spacecraft remains close to the intended GT-1 region. However, in the $+90$- deg case, the energy varies widely, and the satellite does not maintain GT-1. This behavior can be attributed to the sign changes that $\cos(\Omega')$ makes around ± 90 deg. At -90 deg, the sign of the cosine function switches in such a way to push the orbital energy back toward its nominal value. At $+90$ deg, the opposite happens. Essentially, $\Omega' = -90$ deg is a stable equilibrium and $\Omega' = +90$ deg is an unstable equilibrium.

Solutions near $\Omega' = -90$ deg remain bounded, but periodic, in the quantity Ω'. The error in Ω' increases as the initial value of Ω' gets further from -90 deg, until the system becomes unstable at $\Omega' = 0$ or 180 deg. For the LAO GT-1 concept to be a viable application, a nearly constant arbitrary value of Ω' should be maintainable. However, due to symmetry of the polar orbit, a range of only 180 deg of Ω' allows for full longitudinal coverage. Thus, only the bounded-error cases of 180 deg $< \Omega' \leq 360$ deg must be considered. The next section describes how one might modulate the charge as part of a feedback-control scheme to compensate for this error in the open-loop dynamics.

B. Recovery of GT-1 Using a Nonconstant Charge

To recover GT-1 behavior under the influences of a tilted-dipole magnetic field, a scheme of charge modulation is developed. Again, the goal is to find a time-varying charge-to-mass ratio that forces a tilted-dipole LAO to track these nontilted solutions. First, the nontilted field solution is further developed analytically. These analytical solutions provide a desired path to track in the tilted-dipole case. Rewriting Eqs. (14) and (20) using the charge-to-mass ratio in Eq. (23) gives

$$\dot{E}_D = -\omega_E \sqrt{a\mu} \sin 2u \tag{45}$$

$$\dot{\Omega}_D = \omega_E - \omega_E \cos 2u \tag{46}$$

where the subscript D refers to a desired quantity.

The rates of energy and right-ascension change must be matched with the desired rates. Equations (41) and (42) are used, with the eccentricity set to zero. Simulations show that the eccentricity of an initially circular orbit remains small even as a GT-1 orbit is attempted. This simplification gives

$$\dot{E} = \frac{q}{m} AL + \frac{q}{m} AL \cos 2u + \frac{q}{m} AM \sin 2u \tag{47}$$

$$\dot{\Omega} = \frac{q}{m} CM - \frac{q}{m} CM \cos 2u + \frac{q}{m} CL \sin 2u \tag{48}$$

with the following definitions:

$$A = \omega_E B_0 \sqrt{\mu} a^{-5/2} \sin i \tag{49}$$

$$C = -\frac{B_0}{a^3 \sin i}\left(1 + \frac{\omega_E}{\sqrt{\mu}} a^{3/2} \cos i\right) \tag{50}$$

$$L = \cos(\Omega_m - \Omega) \sin \alpha \tag{51}$$

$$M = \sin(\Omega_m - \Omega) \cos i \sin \alpha + \sin i \cos \alpha \tag{52}$$

Noting how Eqs. (47) and (48) depend on the argument of latitude u, we define a charge-to-mass ratio with the same frequency dependencies:

$$\frac{q}{m} = k_1 + k_2 \sin 2u + k_3 \cos 2u \tag{53}$$

Thus, q/m has a constant baseline with a sinusoidal curve superimposed.

Substituting the charge-to-mass in Eq. (53) into Eqs. (47) and (48) yields

$$\begin{aligned}\dot{E} = {} & (k_1 AL + \tfrac{1}{2} k_2 AM + \tfrac{1}{2} k_3 AL) + (k_1 AM + k_2 AL) \sin 2u \\ & + (k_1 AL + k_3 AL) \cos 2u + (\tfrac{1}{2} k_2 AL + \tfrac{1}{2} k_3 AM) \sin 4u \\ & + (-\tfrac{1}{2} k_2 AM + \tfrac{1}{2} k_3 AL) \cos 4u\end{aligned} \tag{54}$$

$$\begin{aligned}\dot{\Omega} = {} & (k_1 CM + \tfrac{1}{2} k_2 CL - \tfrac{1}{2} k_3 CM) + (k_1 CL - k_2 CM) \sin 2u \\ & + (k_1 CL + k_3 CM) \cos 2u + (-\tfrac{1}{2} k_2 CM + \tfrac{1}{2} k_3 CL) \sin 4u \\ & + (-\tfrac{1}{2} k_2 CL - \tfrac{1}{2} k_3 CM) \cos 4u\end{aligned} \tag{55}$$

These two expressions, Eqs. (54) and (55), are set equal to the desired rates of change given in Eqs. (45) and (46), respectively. For these equalities to always hold true, each frequency component in both the energy and right-ascension expressions must equate to its counterpart in the desired track equation. Between the two different expression, there are 10 different conditions (i.e., two each for the $\sin 2u$, $\cos 2u$, $\sin 4u$, $\cos 4u$, and constant terms).

Because there are 10 linear equations for only three unknowns (k_1, k_2, and k_3), the system is overdetermined. The system can be solved with a least-squares regression; however, not all can be satisfied simultaneously, resulting in an imperfect solution. Instead, we choose to solve a full-rank square subspace of the 10 equations. Three equations concisely capture the desired behavior. The most important conditions are the constant term of $\dot{\Omega}$ to ensure GT-1 behavior and the constant and first sine term of the $\dot{E}$ to keep the orbit near its nominal state. Thus, the linear system that is solved for each coefficient is given by

$$\begin{bmatrix} AM & \frac{1}{2}AM & \frac{1}{2}AL \\ AM & AL & 0 \\ CM & \frac{1}{2}CL & -\frac{1}{2}CM \end{bmatrix} \begin{bmatrix} k_1 \\ k_2 \\ k_3 \end{bmatrix} = \begin{bmatrix} 0 \\ -\omega_E^2 \sqrt{a\mu} \\ \omega_E \end{bmatrix} \tag{56}$$

The solution of Eq. (56) is substituted into Eq. (53) to obtain a value of q/m at a given point in the orbit.

If A, C, L, and M are treated as constants, which assumes Ω changes exactly with the rotation of the Earth and the other orbital elements are constant, the system in Eq. (56) can be solved analytically. Carrying out this solution yields the desired coefficients for defining the charge-to-mass ratio as

$$\begin{aligned} k1 &= \frac{\omega_E(\omega_E \sqrt{a\mu} CM^2 + \omega_E \sqrt{a\mu} CL^2 + 2AL^2)}{ACM(3L^2 - M^2)} \\ k2 &= \frac{-2(A + 2\omega_E \sqrt{a\mu} C)\omega_E L}{ACM(3L^2 - M^2)} \\ k3 &= \frac{-2\omega_E(2AL^2 - AM^2 + \omega_E \sqrt{a\mu} CL^2 - \omega_E \sqrt{a\mu} CM^2)}{ACM(3L^2 - M^2)} \end{aligned} \tag{57}$$

In principle, the coefficients in Eq. (53) will reproduce GT-1 behavior under a tilted-dipole magnetic field. However, this scheme is open-loop and the resulting system is not guaranteed to be stable.

Figure 12 shows the results of a simulation using the charge-to-mass ratio calculated by Eqs. (53) and (57). All simulations in this section begin at a time at which Earth-centered and inertial longitudes are equal. The magnetic north pole is placed at its physical location ($\alpha = 10$ deg and $\Omega_m = -114$ deg). In Fig. 12, the top plot shows the error in right-ascension angle in degrees over 15 days. The lower plot shows the error in specific energy in m^2/s^2 over the same time period. The desired average right ascension for this simulation is 0 deg, with the desired average energy corresponding to a 400-km-alt circular orbit. Using the solution of Eq. (57) and the parameters of this simulation, q/m varies from about 2.5 to 3.3 C/kg.

For comparison, Fig. 13 shows the results of a simulation under the same initial conditions using a constant charge-to-mass ratio ($q/m = 2.93$). The same two plots are shown. The comparison of these two figures shows that the charge-varying scheme greatly reduces the errors in right ascension and energy. For a constant charge-to-mass ratio, the maximum right-ascension error is 51.68 deg. Under the open-loop-varying scheme, the maximum error is only 4.76 deg. However, the error in the varying charge does not asymptotically approach zero or fall into a periodic motion, and

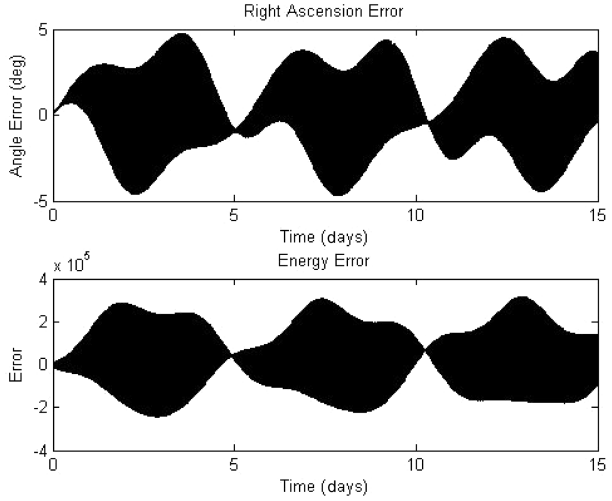

Fig. 12 Right ascension and energy error over 15 days for a spacecraft using the variable charge-to-mass scheme defined in Eqs. (53) and (57). The desired average right ascension is 0 deg. The orbit is initially a 400-km-alt circle. The geomagnetic field is tilted to 10 deg.

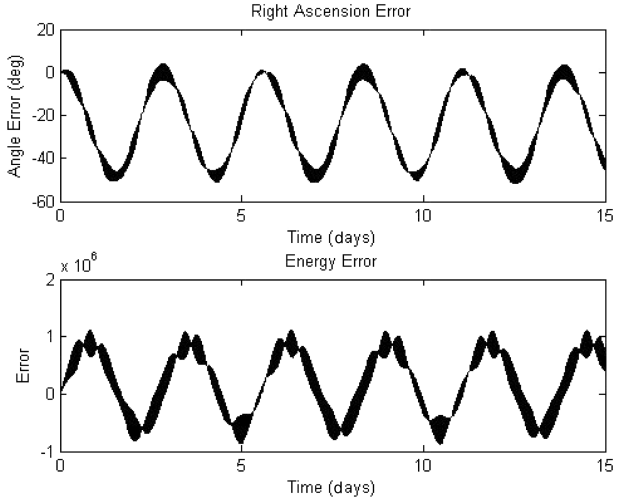

Fig. 13 Right ascension and energy error over 15 days for a spacecraft under a constant charge. The desired average right ascension is 0 deg. The orbit is initially a 400-km-alt circle. The geomagnetic field is tilted to 10 deg.

so its stability is not guaranteed. To enforce a guarantee, feedback control is introduced.

C. Feedback Control for q/m

Although the open-loop solution generally reproduces GT-1 behavior over short time scales, the resulting system is open-loop and is prone to instabilities due to imperfect modeling. To remedy this situation, feedback is introduced to the expression defining q/m:

$$\frac{q}{m} = k_1 + k_2 \sin 2u + k_3 \cos 2u + k_4(\Omega - \Omega_D) + k_5(E - E_D) \tag{58}$$

where k_1, k_2, and k_3 are as given in Eq. (57), and Ω_D and E_D are defined by integrating Eqs. (45) and (46), respectively. Thus, k_4 and k_5 are feedback gains and the Ω and E terms are errors to be zeroed. The definition of q/m in Eq. (58) is substituted into Eqs. (47) and (48). The terms involving k_1, k_2, and k_3 are assumed to satisfy the 10-equation system defined by Eqs. (54) and (55). This assumption is not explicitly true, because k_1, k_2, and k_3 are only chosen to satisfy Eq. (56), but the resulting error can be treated as a small unmodeled disturbance. Applying this assumption gives

$$\dot{\Omega} = \dot{\Omega}_D + (CM - CM\cos 2u + CL \sin 2u)[k_4(\Omega - \Omega_D) + k_5(E - E_D)] \tag{59}$$

$$\dot{E} = \dot{E}_D + (AL + AL\cos 2u + AM \sin 2u)[k_4(\Omega - \Omega_D) + k_5(E - E_D)] \tag{60}$$

Combining these equations (59) and (60) into a state-space system yields

$$\begin{bmatrix} \dot{\Omega} - \dot{\Omega}_D \\ \dot{E} - \dot{E}_D \end{bmatrix} = \begin{bmatrix} k_4 C(M - M\cos 2u + L\sin 2u) & k_5 C(M - M\cos 2u + L\sin 2u) \\ k_4 A(L + L\cos 2u + M\sin 2u) & k_5 A(L + L\cos 2u + M\sin 2u) \end{bmatrix} \times \begin{bmatrix} \Omega - \Omega_D \\ E - E_D \end{bmatrix} \tag{61}$$

Equation (61) represents a closed-loop, linear, time-varying (LTV) system. Describing the stability of an LTV system is not as simple or straightforward as the time-invariant case. The eigenvalues of the state matrix being in the left-half plane is neither a sufficient nor necessary condition of stability. However, if the state matrix changes sufficiently slowly in time, the state matrix being Hurwitz can show stability. Rosenbrock [20] puts explicit bounds on the rate of change of the state matrix. We do not develop specific bounds in the method of Rosenbrock, but use the eigenvalues of the state matrix as a guide to selecting a controller, which will later be shown numerically to be stable based on the state transition matrix.

Solving for the eigenvalues yields the following condition on the gains k_4 and k_5:

$$k_5 < -k_4 \frac{C(M - M\cos 2u + L \sin 2u)}{A(L + L\cos 2u + M \sin 2u)} \tag{62}$$

Gains that meet the criterion in Eq. (62) give the system a negative real eigenvalue. The second eigenvalue of system is always zero. Using Eq. (62) as a guideline, a stabilizing controller is found to be

$$k_4 = -0.5 \qquad k_5 = \frac{-k_4 C(M - M\cos 2u + L \sin 2u) + (k_4 - 0.05)\|C(M - M\cos 2u + L \sin 2u)\|}{A(L + L\cos 2u + M \sin 2u)} \tag{63}$$

where the symbol $\|(\cdot)\|$ refers to absolute value. The gain k_5 is not constant. This set of gains results in stable errors in energy and right ascension over at least 180 deg of desired average right-ascension angle in simulation, implying that any Earth-fixed longitude can be tracked in GT-1 fashion with bounded finite error.

The results of the controller in Eq. (63) are explored numerically. Figure 14 shows right ascension and energy error under the same conditions as the simulations shown in Figs. 12 and 13. The feedback-control scheme uses about the same range of q/m values as the open-loop scheme. The maximum right-ascension error of the feedback case is 4.12 deg, less than the open-loop error of 4.76 deg. Additionally, the error in the feedback case falls into a periodic motion and is stable for all time.

The plots shown in Fig. 15 are intended to demonstrate the improvement in stability of the feedback-control scheme over the open-loop variable q/m case. Figure 15a shows the results of an open-loop simulation similar to those done previously, but with a desired average ascension angle of 70 deg. This orbit deviates widely from the desired path. The system in this case is unstable. Figure 15b shows the same simulation using the feedback controller. The controller is able to stabilize the system, and results in bounded error. Despite the large error bounds, the underlying system is stable.

Figure 16 further elucidates the stable periodic nature of the feedback solution. This figure shows the right ascension and energy error under feedback control for a circular 400-km orbit with desired average right ascension of 45 deg. This simulation is carried out for 75 days, and the periodic nature of the error is evident.

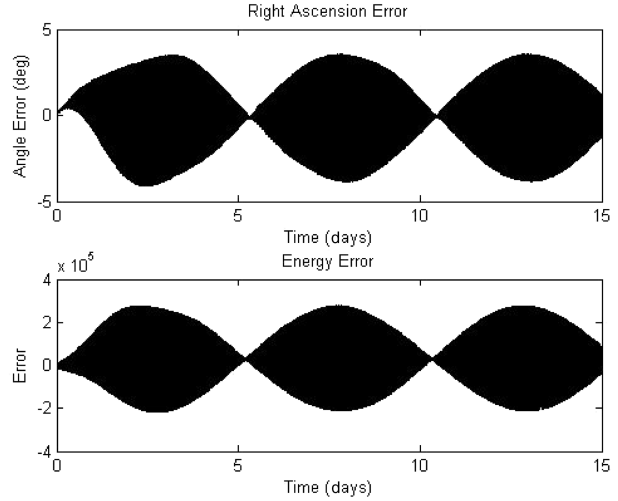

Fig. 14 Right ascension and energy error over 15 days for a spacecraft using the feedback-control scheme defined in Eq. (58). The desired average right ascension is 0 deg. The orbit is initially a 400-km-alt circle. The geomagnetic field is tilted to 10 deg.

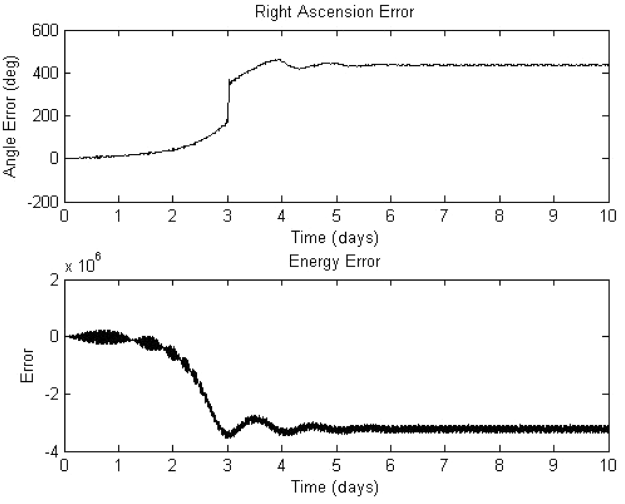

a) Open-loop scheme

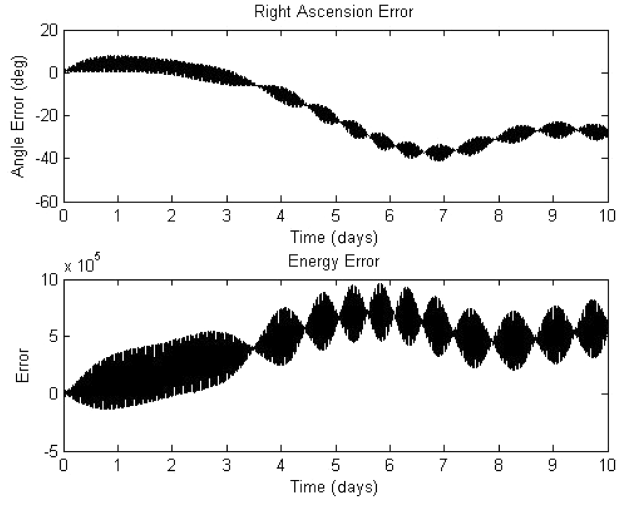

b) Feedback scheme

Fig. 15 Right ascension and energy error over 15 days for a spacecraft using the open-loop scheme and the feedback controller. The desired average right ascension is 70 deg. The orbit is initially a 400-km-alt circle. The geomagnetic field is tilted to 10 deg.

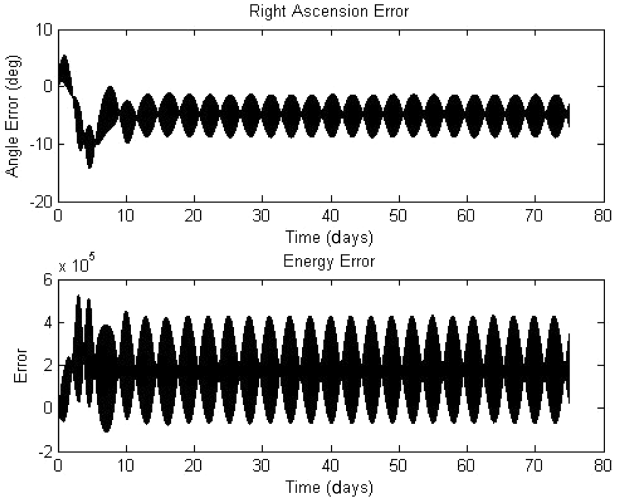

Fig. 16 Right ascension and energy error over 75 days for a spacecraft using the feedback-control scheme defined in Eq. (58). The desired average right ascension is 45 deg. The orbit is initially a 400-km-alt circle. The geomagnetic field is tilted to 10 deg.

To show numerically that the controller in Eq. (63) does indeed stabilize the system in Eq. (61), we use the result that an LTV system is stable if and only if the norm of its state transition matrix is bounded for all time [21]. We numerically solve for the state transition matrix $\Phi(t, 0)$ for the system simulated in Fig. 16. Given the time history of this simulation, the system matrix of Eq. (61) can be found as a function of time. Two linearly independent initial conditions, x_{0_1} and x_{0_2} are then integrated using the system matrix. With the two resulting time histories, $x_1(t)$ and $x_2(t)$, the state transition matrix is given by

$$\Phi(t, 0) = [x_1(t) \;\; x_2(t)][x_{0_1} \;\; x_{0_2}]^{-1} \tag{64}$$

Figure 17 shows the matrix-induced 2-norm of the state transition matrix. Because the norm is bounded, the system is stable. However, the result in Fig. 17 does not give uniform stability of the system, nor does it prove that the system is stable over a range of desired right-ascension values. The norm of $\Phi(t, 0)$ approaching zero as time increases leads to the conclusion that Eq. (61) is asymptotically stable, but the error plots in Fig. 16 plainly show errors approaching some nonzero value. In Fig. 16, the linear system in Eq. (61) is not being simulated, but the full nonlinear system of Eqs. (6–8).

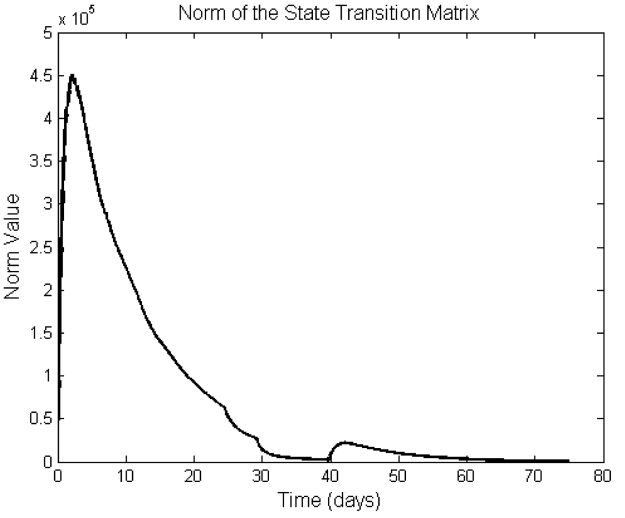

Fig. 17 Matrix norm of the state transition matrix of the system in Eq. (61), using data from the simulation shown in Fig. 16.

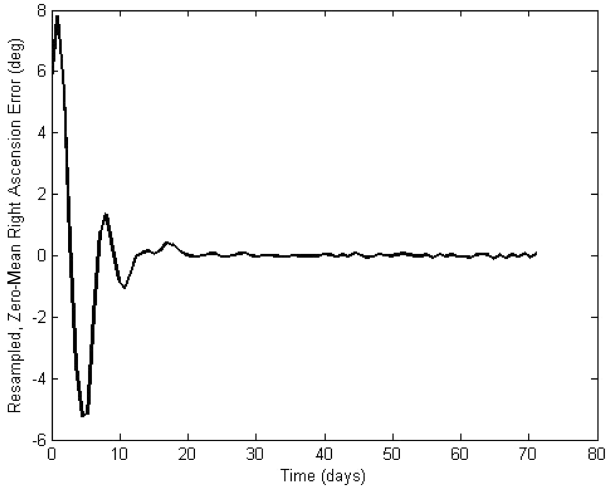

Fig. 18 Resampled right-ascension error over 75 days for the simulation displayed in Fig. 16. The actual right-ascension error is Fourier-transformed. The power spectral density of this transform is used to find the two main frequencies present, and the error is numerically resampled at the difference between these frequencies. The long-term average error is also subtracted to create a zero-mean system.

Assumptions made in deriving Eq. (61) cause it to be not entirely accurate.

However, we show numerically that the full nonlinear solution still approaches a stable and periodic nonzero error. Figure 18 is used to more rigorously show the periodicity of the right-ascension error in Fig. 16. At first glance, the long-term behavior of the error appears to be a periodic beat of two similar frequencies. To test this hypothesis, the error data are transformed to the frequency domain. The power spectral density of this transform shows two distinct peaks. One peak occurs at a frequency near twice per orbit; the other occurs at slightly less than twice per orbit. The data are numerically resampled at the beat frequency of the two frequency peaks. The long-term average right-ascension error is subtracted from the resampled data, and the resulting curve is plotted in Fig. 18. As the transient response damps out, this curve goes to zero, indicating good agreement with the periodic beating assumption.

The feedback controller presented in Eq. (58) with the gains in Eq. (63) stabilizes GT-1 behavior under the influence of a tilted geomagnetic field. This controller consists of proportional feedback based on a linearized model and does not guarantee asymptotic convergence. However, the controller does bound the error in right ascension and energy. Numerical analysis shows that the system is stabilized for a full range of desired average right ascensions and initial orbit altitudes.

VI. Conclusions

Lorentz-augmented orbits (LAOs) are based on simple physical principles but can be used to accomplish a variety of complex orbital behaviors. Analytical results, verified by numerical simulations, show the effects of the Lorentz force on the orbit of an LAO satellite. The resulting changes in orbital elements can be used to develop novel applications. These new applications include polar single-orbit repeat-groundtrack (GT-1) satellites. A successfully implemented GT-1 LAO orbit would greatly outperform today's imaging satellites. These orbits can exist at any altitude, not just the traditional geosynchronous height. We have derived from first principles a simple expression for the charge required to achieve such an orbit. This expression is verified numerically and allows for mission designs to be evaluated. Also numerically confirmed is the existence of equatorial orbits with arbitrary control over the location of perigee. Again, a simple expression for the charge required is shown from first principles. These orbits can create an Earth-synchronous orbit for which the perigee and apogee lie at a constant longitude.

The presence of a tilt in the Earth's magnetic field greatly complicates GT-1 behavior. The GT-1 orbit in this case is not stable for constant charge. However, modulating the charge as a means of feedback control is shown to stabilize a GT-1 LAO. The addition of controlled nonconstant charge opens many new avenues in LAO research, including orbit raising, inclination change, flyby augmentation, rendezvous, and formation control.

Acknowledgments

This work was supported by the NASA Institute for Advanced Concepts and the National Science Foundation's Integrative Graduate Education and Research Traineeship (IGERT) Program in Nonlinear Systems at Cornell University.

References

[1] Wertz, J. R., and Larson, W. J., *Space Mission Analysis and Design*, Microcosm Press, El Segundo, CA, 1999, pp. 141–156.

[2] Peck, M. A., "Prospects and Challenges for Lorentz-Augmented Orbits," AIAA Guidance, Navigation, and Control Conference, San Francisco, CA, AIAA Paper 2005-5995, Aug. 2005.

[3] Cosmo, M. L., and Lorenzini, E. C., *Tethers in Space Handbook Third Edition*, NASA Marshall Spaceflight Center, Huntsville, AL, 1997, pp. 119–151.

[4] Rothwell, P. L., "The Superposition of Rotating and Stationary Magnetic Sources: Implications for the Auroral Region," *Physics of Plasmas*, Vol. 10, No. 7, 2003, pp. 2971–2977. doi:10.1063/1.1582473

[5] Schaffer, L., and Burns, J. A., "The Dynamics of Weakly Charged Dust: Motion Through Jupiter's Gravitational and Magnetic Fields," *Journal of Geophysical Research*, Vol. 92, Mar. 1987, pp. 2264–2280.

[6] Schaffer, L., and Burns, J. A., "Charged Dust in Planetary Magnetospheres: Hamiltonian Dynamics and Numerical Simulations for Highly Charged Grains," *Journal of Geophysical Research*, Vol. 99, No. A9, 1994, pp. 17211–17223. doi:10.1029/94JA01231

[7] Hamilton, D. P., "Motion of Dust in a Planetary Magnetosphere: Orbit-Averaged Equations for Oblateness, Electromagnetic, and Radiation Forces with Applications to Saturn's F Ring," *Icarus*, Vol. 101, No. 2, Feb. 1993, pp. 244–264. doi:10.1006/icar.1993.1022Erratum: *Icarus*, Vol. 103, No. 1, May 1993, p. 161. doi:10.1006/icar.1993.1065

[8] Mullen, E. G., Gussenhoven, M. S., and Hardy, D. A., "SCATHA Survey of High-Level Spacecraft Charging in Sunlight,"*Journal of Geophysical Research*, Vol. 91, No. A2, 1986, pp. 1474–1490.

[9] Garrett, H. B., and Whittlesey, A. C., "Spacecraft Charging: An Update," *IEEE Transactions on Plasma Science*, Vol. 28, No. 6, 2000, pp. 2017–2028. doi:10.1109/27.902229

[10] Schaub, H., Parker, G. G., and King, L. B., "Challenges and Prospects of Coulomb Spacecraft Formations," AAS John L. Junkins Symposium, College Station, TX, American Astronautical Society Paper 03-278, May 2003.

[11] Lai, S. T., "An Overview of Electron and Ion Beam Effects in Charging and Discharging of Spacecraft," *IEEE Transactions on Nuclear Science*, Vol. 36, No. 6, 1989, pp. 2027–2032. doi:10.1109/23.45401

[12] Hough, M. E., "Lorentz Force Perturbations of A Charged Ballistic Missile," AIAA Guidance and Control Conference, San Diego, CA, AIAA Paper 1982-1549, Aug. 1982.

[13] King, L. B., Parker, G. G., Deshmukh, S., and Chong, J., "A Study of Inter-Spacecraft Coulomb Forces and Implications for Formation Flying," AIAA Joint Propulsion Conference, Indianapolis, IN, AIAA Paper 2002-3671, July 2002.

[14] Schaub, H., "Stabilization of Satellite Motion Relative to a Coulomb Spacecraft Formation," *Journal of Guidance, Control, and Dynamics*, Vol. 28, No. 6, 2005, pp. 1231–1239.

[15] Bergamin, L., Izzo, D., and Pinchook, A., "Propellantless Propulsion in Magnetic Fields by Partially Shielded Current," International Astronautical Congress Paper 06-C4.6.05, 2006.

[16] Tikhonov, A. A., "A Method of Semipassive Attitude Stabilization of a Spacecraft in the Geomagnetic Field," *Cosmic Research (Translation of Kosmicheskie Issledovaniya)*, Vol. 41, No. 1, 2003, pp. 63–73. doi:10.1023/A:1022355730291

[17] Van de Graaf, R. J., Compton, K. T., and Van Atta, L. C., "The Electrostatic Production of High Voltage for Nuclear Investigations," *Physical Review*, Vol. 43, No. 3, 1933, pp. 149–157.
doi:10.1103/PhysRev.43.149

[18] Burns, J. A., "Elementary Derivation of the Perturbation Equations of Celestial Mechanics," *American Journal of Physics*, Vol. 44, No. 10, 1976, pp. 944–949.
doi:10.1119/1.10237

[19] Atchison, J., Streetman, B., and Peck, M. A., "Prospects for Lorentz Augmentation in Jovian Captures," AIAA Guidance, Navigation, and Control Conference, Keystone, CO, AIAA Paper 2006-6596, Aug. 2006.

[20] Rosenbrock, H. H., "The Stability of Linear Time-Dependent Control Systems," *Journal of Electronics and Control*, Vol. 15, No. 1, 1963, pp. 73–80.

[21] Willems, J. L., *Stability Theory of Dynamical Systems*, Wiley, New York, 1970.